Received May 1996
Revised October 1996
Accepted September 1997

Numerical and experimental study of inclined open thermosyphons

F. O. Gaa, M. Behnia, S. Leong and G. L. Morrison
School of Mechanical and Manufacturing Engineering, The University of New South Wales, Sydney, Australia

Introduction

The thermosyphon effect is achieved when heat is transported between two objects by means of the natural convection of a fluid under the influence of a body force. Japikse (1972) reviewed the use of this effect in gas turbine blade cooling, transformer cooling and cooling of nuclear reactor. It is also commonly used in evacuated tubular solar water heaters (Chow *et al.,* 1984). Evacuated tubular solar absorbers are basically long cylinders whose bottom end is sealed and whose top is connected to a reservoir. Under exposure to the sun natural convection currents are generated within the cylinder, driving an exchange of fluid as well as heat between the absorber tube and the reservoir.

The present work, which aims to investigate the flow of water inside such enclosures, is made up of two parts: the numerical model and experimental observations. The numerical model consists of the solution of the equations of conservation of mass, momentum and energy, by means of a finite difference iterative algorithm. The solution domain is a cylindrical cavity with heated walls, whose bottom is sealed and whose top is open to a uniform temperature reservoir. Since the reservoir is not part of the domain, special boundary conditions are required for the open end of the cylinder so that the mass transfer into and out of the cylinder can be simulated.

Abib and Jaluria (1988) reported a two-dimensional solution of flow inside a partially open cavity, using the vorticity-stream function formulation of the governing equations. They assumed that the entry and exit velocities at the open end were normal to the opening and that the gradient in the normal direction was zero, which is like fully developed flow. They made the same assumption (i.e. fully developed in the outward normal direction) about all other variables on that surface, including vorticity and stream function. For three-dimensional domains such as the present problem, a generalised solution was developed by Hirasaki and Hellums (1967) for the vector potential on any surface, solid or flow-through. This involved the introduction of an auxiliary vector $\tilde{B}$ whose surface curl gives the tangential components of the vector potential on the surface. The present work is an extension of their approach, in that their generalised formula is re-worked in cylindrical coordinates and applied to a surface, which has both inflow and outflow.

International Journal of Numerical Methods for Heat & Fluid Flow
Vol. 8 No. 7, 1998, pp. 748–767.

Solutions are generated for various combinations of Rayleigh number, aspect ratio and mode of heating. Rayleigh number ranges from 10^3 to 10^6, aspect ratio (L/R_0) from 10 to 50 and two heating configurations. Either the wall temperature is set to a uniform value all around the sides of the cylinder (uniform wall heating, UWH); or one uniform temperature is applied on the upper surface (which normally faces the sun in a typical solar absorber) and another uniform temperature on the lower surface (which normally faces a reflective panel). The latter mode of heating, called differential wall heating (DWH), is the more relevant form of heating in the solar application. Tubes used in evacuated tubular solar collectors are typically 1m long and 30 to 50mm in diameter. The tubes are spaced apart by one to two diameters with a reflecting surface behind the tubes. With this configuration the top and back of the tubes are heated, however, the top surface which is exposed directly to the sun usually receives higher radiant energy input.

The experimental part of the work involves the measurement of flow in an artificially heated inclined thermosyphon. Similar aspect ratios and heating conditions as in the numerical model were used but the Rayleigh number was limited to approximately 10^6. Measurement of axial velocity was done at the orifice by means of laser doppler anemometry. Flow visualisation has been reported by Behnia *et al.* (1987) on a similar experimental rig. They traced the flow inside the thermosyphon by introducing dye and tracer particles and made temperature measurements on the central vertical plane by inserting a movable multi-sensor thermocouple rake into the tube. The LDA measurements in the present investigation gave the axial velocity profiles at the orifice, which were compared with the results of the numerical model.

Numerical model

The numerical model simulates the flow in a cylinder as shown in Figure 1. The heated sides are non-slip impermeable walls. The bottom is also a solid non-slip wall but is adiabatic. The top allows inflow and outflow to the reservoir. Incoming fluid is assumed to have the temperature of the reservoir, while outgoing fluid is assumed to have zero axial temperature gradient in the z-direction. The velocity at the orifice is assumed to have no transverse components (i.e. $u = v = 0$) which gives $\partial w/\partial z = 0$ for the continuity equation to be satisfied there. Boundary conditions of vorticity and vector potential are discussed in detail below.

Governing equations

The non-dimensional vorticity transport and energy equations governing buoyancy driven laminar flow are as follows

$$\frac{\partial \vec{\zeta}}{\partial t} - \nabla \times \left(\vec{u} \times \vec{\zeta} \right) = -Ra \, \mathrm{Pr} \, \nabla \times \theta \vec{g} - \mathrm{Pr} \, \nabla \times \left(\nabla \times \vec{\zeta} \right) \tag{1}$$

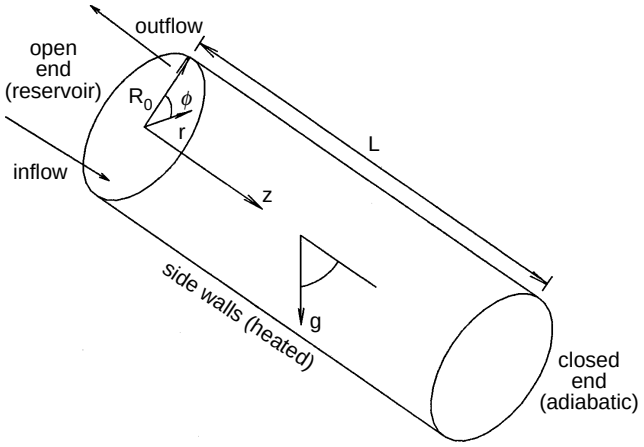

Figure 1.
Cylindrical domain of numerical solution, open top leads to reservoir

$$\frac{\partial \theta}{\partial t} = -(\tilde{u} \cdot \nabla)\theta + \nabla^2 \theta \tag{2}$$

$$\zeta = \nabla \times (\nabla \times \tilde{\psi}) \tag{3}$$

where Pr is the Prandtl number defined as ν/κ and Ra is the Rayleigh number $\beta g \Delta T R_0^3 \mathrm{Pr}/\nu^2$. These equations were solved for the steady-state condition. The non-dimensional velocity, length, time and temperature are defined as follows:

$$u = \frac{u'}{V}, \quad r = \frac{r'}{R_0}, \quad z = \frac{z'}{R_0}, \quad t = \frac{t'}{t^*}, \quad \theta = \frac{T - T_{av}}{\Delta T}$$

where V, R_0 and t^* are scale factors and $T_{av} = \frac{1}{2}(T_{hot} + T_{cold})$ and $\Delta T = \frac{1}{2}(T_{hot} - T_{cold})$. T_{hot} is the temperature of the heated upper half of the curved cylindrical wall and T_{cold} is the temperature of the lower half of the curved cylindrical wall. The term β is the volumetric coefficient of expansion, T the temperature, $\tilde{g}$ the gravity vector, ν the kinematic viscosity and κ the thermal diffusivity.

The scale factor V for velocity is obtained by equating the coefficients of the advection term and the thermal diffusion term in the energy equation to give $V = \kappa/R_o$

And to ensure that the thermal diffusion term will be of unit order of magnitude, we use $t^* = R_0^2/\kappa$.

Boundary conditions (impermeable walls)

The sides of the cylinder and the bottom end are impermeable non-slip walls and therefore all components of velocity are zero there. One temperature θ_{hot} is specified on the entire sidewall in uniform wall heating mode. In differential wall heating, θ_{hot} is specified on the upper surface of the cylinder wall and θ_{cold}

on the lower. The bottom end is assumed to be adiabatic therefore $\partial\theta/\partial z$ is zero there. The heated wall boundary condition is $\theta = 1$ and in the case of differential heating the lower wall boundary condition is $\theta = 0$.

Boundary conditions for vector potential are similar to those of Hirasaki and Hellums (1967), that is on the curved walls

$$\psi_z = \psi_\phi = \frac{\partial(r\psi_r)}{\partial r} = 0 \tag{4}$$

and on the bottom end wall

$$\psi_r = \psi_\phi = \frac{\partial \psi_z}{\partial z} = 0 \tag{5}.$$

The boundary conditions for vorticity are presented here without discussion as their derivation is quite lengthy but they are based on the assumption that vorticity varies linearly within the first interval from wall (a complete derivation is given by Leong (1981)). At the end wall the following boundary conditions apply:

$$\zeta_{r,N} = -\frac{3}{\Delta z^2}\psi_{r,N-1} - \frac{3}{\Delta z}\frac{\partial \psi_z}{\partial r}\bigg|_N - \frac{\zeta_{r,N-1}}{2} \tag{6}$$

$$\zeta_{\phi,N} = -\frac{3}{\Delta z^2}\psi_{\phi,N-1} - \frac{1}{r}\frac{3}{\Delta z}\frac{\partial \psi_z}{\partial \phi}\bigg|_N - \frac{\zeta_{\phi,N-1}}{2} \tag{7}$$

and

$$\zeta_{z,N} = 0 \tag{8}$$

where N is the number of nodes in the z-direction. On the sidewalls the same method is used to determine the boundary values of vorticity.

Boundary conditions (flow-through surface)

It is assumed that the fluid entering the thermosyphon is at the reservoir temperature. All fluid going out is assumed to have a fully developed temperature distribution, i.e. $\partial\theta/\partial z = 0$. At the orifice all transverse components of velocity (i.e. u and v) are assumed to be zero, therefore in order to satisfy continuity there, we have $\partial w/\partial z = 0$.

The vorticity boundary condition at the orifice cannot be derived in the same manner as with impermeable walls because the tangential components of vector potential are no longer zero there. The most convenient way of specifying vorticity on the open surface ($k = 1$) is by using the definition of vorticity in terms of velocity:

$$\zeta_r\big|_{k=1} = \frac{1}{r}\frac{\partial w}{\partial \phi} - \frac{\partial v}{\partial z} \tag{9}$$

$$\zeta_\phi\big|_{k=1} = \frac{\partial u}{\partial z} - \frac{\partial w}{\partial r} \tag{10}$$

$$\zeta_z\big|_{k=1} = 0 \tag{11}$$

since $u = v = 0$ on this surface. The first node in the z-direction is denoted by $k = 1$.

For the solution of vector potential at the open surface, we introduce an auxiliary vector $\tilde{B}$, whose surface curl gives the tangential components of vector potential.

$$\tilde{\psi}_t = \nabla_s \times \tilde{B} \tag{12}$$

This vector $\tilde{B}$ exists only on the open surface and does not extend to the interior points. It is also assumed to have no tangential components on the r-ϕ plane hence $\tilde{B} = (0,0,B_z\tilde{k})$

Therefore (4) can be expressed as

$$\psi_r = \frac{1}{r}\frac{\partial B_z}{\partial \phi} \tag{13}$$

$$\psi_\phi = -\frac{\partial B_z}{\partial r} \tag{14}$$

By the definition of the vector potential, the relationship between $\tilde{B}$ and the velocity is given by

$$\tilde{u} = \nabla \times \nabla_s \times \tilde{B} \tag{15}$$

This gives a means of determining the distribution of $\tilde{B}$ along the open surface, provided that the velocity is known there. Wong and Reizes (1984) and Yang and Camarero (1986) used a fixed velocity distribution on the orifice in their open duct simulations. They therefore had to solve $\tilde{B}$ only at the beginning of their iterative solution. In the present work, velocity is updated at the orifice at each iteration using $\partial w/\partial z = 0$, and $\tilde{B}$ therefore is likewise progressively updated.

Since the transverse components of $\tilde{u}$ and $\tilde{B}$ are zero, equation (15) reduces to

$$w = -\frac{1}{r}\frac{\partial B_z}{\partial r} - \frac{\partial^2 B_z}{\partial r^2} - \frac{1}{r^2}\frac{\partial^2 B_z}{\partial \phi^2} \tag{16}$$

For equation (16) to be solved at the open surface, boundary conditions for B_z must be provided at the edges. Hirasaki and Hellums state that the only requirement for the use of $\tilde{B}$ is that $\tilde{\Psi}$ should be continuous at the adjoining surfaces. Along the sidewalls $\Psi_\phi = 0$, which may be satisfied by equation (14) if

$$\frac{\partial B_z}{\partial r} = 0 \tag{17}$$

The boundary condition for Ψ_r at the sidewalls is $\partial(r\Psi_r)/\partial r = 0$. Again using equation (14) we get

$$\frac{\partial^2 B_z}{\partial r \partial \phi} = 0 \tag{18}$$

If this is integrated over one revolution, then

$$\left.\frac{\partial B_z}{\partial r}\right|_{2\pi} - \left.\frac{\partial B_z}{\partial r}\right|_{0} = 0 \tag{19}$$

which can also be satisfied by equation (17). The third component of vector potential has the same boundary condition whether the surface is impermeable or flow-through, therefore (19) is a sufficient boundary condition for (17) to be solved on the orifice.

Solution procedure

The governing equations (1), (2) and (3) were re-written in cylindrical polar coordinate form and then approximated by finite differences. A mesh size of $31 \times 32 \times 33$ distributed in uniform intervals in the r-, ϕ- and z-directions respectively was used. A more detailed mesh system was investigated and only minor changes were observed in the mass flow in and out of the cylinder. Nodes were not placed on the central axis of the cylinder to avoid the singularity in terms having 1/r for a coefficient. Central spacing is used on spatial derivatives and forward differencing for all time derivatives. The alternating direction implicit (ADI) scheme is used to solve the parabolic equations (1) and (2), with the aid of a false transient factor. Thus the transient path towards convergence cannot be regarded as the true transient solution. For the solution of the elliptic equation (3), the successive over-relaxation (SOR) method is used.

At the beginning of a solution, all field variables ($\tilde{u}$, $\tilde{\Psi}$, $\tilde{\zeta}$ and θ) are set to zero, with the exception of the temperature values at the walls. The solution is obtained in a stepwise iterative manner in time. The temperature at the orifice will depend on whether fluid is incoming or outgoing. Vorticity is solved from equation (1) on all internal points and then at the solid walls using (6) to (8). At the orifice, vorticity is solved from (9) to (11). The vector potential is solved from the vorticity field using (3) at all internal points and using (4) and (5) on the impermeable walls. For the open end equations (13) and (14) are used. The

velocity field is then updated directly from the vector potential but at the orifice, $\partial w/\partial z = 0$ is used. Finally $\tilde{B}$ is solved from the velocity field at the orifice using equation (16) with the SOR method. Convergence is measured by the rate of change of the temperature and vorticity fields within a time step. When the sum of all nodal changes of these variables goes below 10^{-5}, then the solution is assumed to be converged. As the temperature differences used in the experiment were relatively small ($\Delta T < 20K$) the spatial variations of fluid properties, other than density, were not considered.

Experimental investigations

Figure 2 shows the general layout of the experimental rig. The thermosyphon is made up of a glass cylinder (22mm inner diameter, 1,400mm long) which is enclosed over 1,200mm of its length by a perspex heating jacket with upper and lower heating chambers. Two temperature controlled water flows were circulated in the two chambers in order to obtain differential heating. The glass cylinder is sealed on the bottom with a solid perspex plug 80mm long to ensure that it acts like an adiabatic wall. The plug may be positioned anywhere along the tube so that the aspect ratio of the active section of the thermosyphon may be changed. The top of the thermosyphon is connected to a uniform temperature water reservoir, $520 \times 520 \times 760$mm in size.

A laser doppler anemometer was mounted on the same frame as the thermosyphon in order to eliminate all relative movement. The laser beam is split into two beams of equal intensity and then focused inside the thermosyphon. Back-scattered light, which contains the velocity information, is

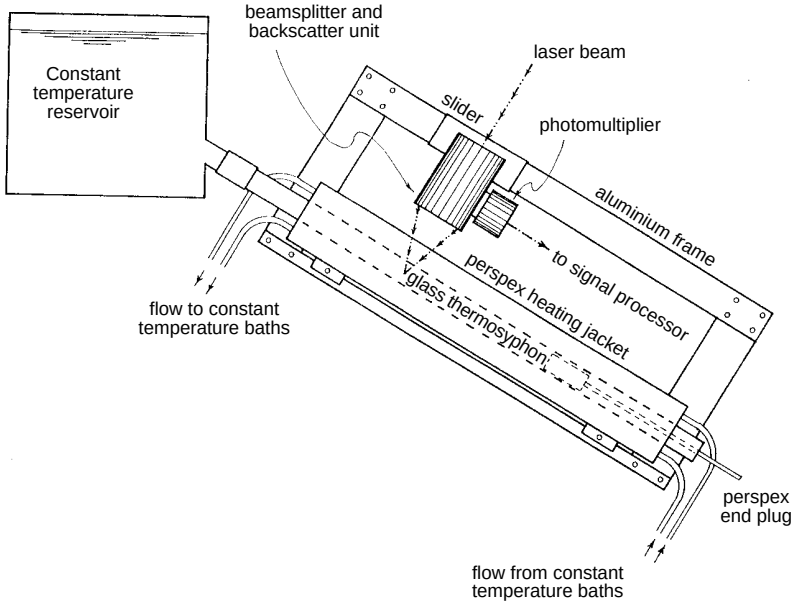

Figure 2.
Experimental test rig

received by a photomultiplier, attached to the beam splitter assembly and is converted into electrical signals. These signals are then filtered and processed by an input conditioner and frequency counter. Visual information is presented to the screen of an oscilloscope and further processing is done by a personal computer, which finally gives the velocity at the measuring point.

The thermosyphon tube and the beam splitter assembly and related optics are carried by a frame whose angle of inclination can be adjusted. This eliminates the need for re-alignment whenever the angle of inclination of the thermosyphon is changed. The splitter assembly sits on a slider, which allows it to traverse the length of the thermosyphon without changing its angle with respect to the incident laser beam, thus allowing measurement of axial velocity on any diameter along the thermosyphon. The entire backscatter unit, which houses the beam splitter, transmitting lens and receiving mirror, sits on a traversing mechanism which allows it to move along the axis of the incoming laser beam. With the traversing mechanism, the focal point of the two beams may be positioned anywhere along a chosen diameter. Diametrical velocity profiles may then be generated. Re-alignment is minimal when tube inclination is changed or when the splitter is traversed down the tube. The operation of the laser system was verified by using it to measure fully developed laminar flow through the test tube.

Experimental procedure

At the beginning of each run the tank is filled with tap water, which contains enough impurities so that artificial seeding for light scattering is not required. For the case of uniform heating, the heating baths for the two chambers are set to the same temperature. In differential heating mode the lower chamber is supplied with water at the reservoir temperature. The characteristic length is the radius (R_o = 0.011m) and the temperature difference is defined as $(T_{hot}-T_{cold})/2$. For a temperature difference of 5K the Rayleigh number is 3.56×10^5. In each run the thermosyphon is allowed to heat up undisturbed until buoyancy-driven motion ensues and reaches steady state. This period normally takes approximately one hour. The difference in the inlet and outlet temperatures of the water flow through the two heating chambers was maintained at less than 0.1K by using high circulation flow rates. This ensured that there was an isothermal outer boundary temperature, however, the inner surface of the glass may not be isothermal due to circumferential conduction through the glass.

The velocity was measured at 12 points over the diameter. Only axial velocity was measured because the azimuthal component was expected to be zero due to symmetry. The radial component was not measured due to obstacles to visibility, such as heating chamber partitions and lengthwise joints separating the two heating chambers. As a laser doppler anemometer provides a vector velocity measurement the presence of azimuthal components of velocity at high Ra does not effect the accuracy of the axial measurements. The orifice was the area of greatest interest, and therefore the profiles were

measured there before anywhere else. Measurements were performed for aspect ratios 10 to 50 at intervals of 10. The point along the cylinder at which the laser measured the velocity was 17.5mm inside the tube, in order to allow the two intersecting laser beams from the beam splitter to reach the measuring point unobstructed.

Numerical results

Uniform wall heating mode

All the numerical results are for an inclination of 45°. Figures 3 and 4 show particle trace lines for an aspect ratio (L/R_0) of ten. Flow at $Ra=10^3$ is made up of two main streams, a cool one going down and a warm one rising up; such flow is called bifilamental. Cooler and heavier fluid from the reservoir enters through the lower half of the orifice cross section, meets the heating surface and immediately rises into the top return stream, thus only a small portion actually reaches the bottom closed end of the cylinder. Most of the cool stream breaks up into smaller filaments which fan out to the side walls and are directed up to the hot return stream on the top wall of the cylinder. For a Ra of 10^6 upward moving streams are strong enough to cause interference at the orifice. Heating is applied all around and therefore some hot streams generated below the cool core rise up in the middle and interfere with the incoming stream. This interaction causes the formation of a secondary flow at the orifice: a portion of the incoming cold stream short circuits back to the reservoir soon after entering the orifice. The same interaction between warm and cool streams may be observed at higher Ra with the same aspect ratio. These computational results are generally supported by the observations of Behnia *et al.* (1987).

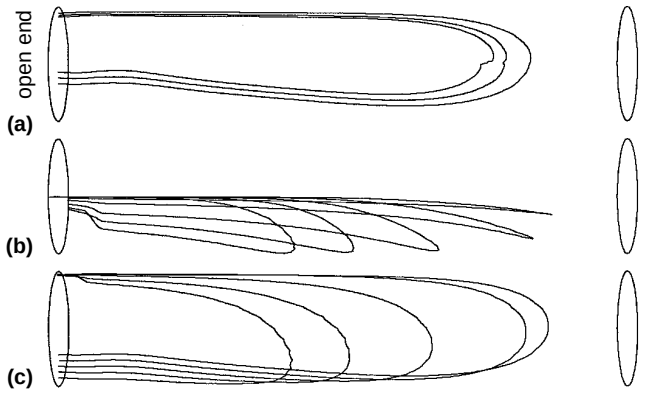

Figure 3.
Particle tracks for uniform wall heating, $Ra = 10^3$, $L/R_0 = 10$.

(a) side view, central vertical plane,
(b) top view, side wall flow,
(c) side view, side wall flow.

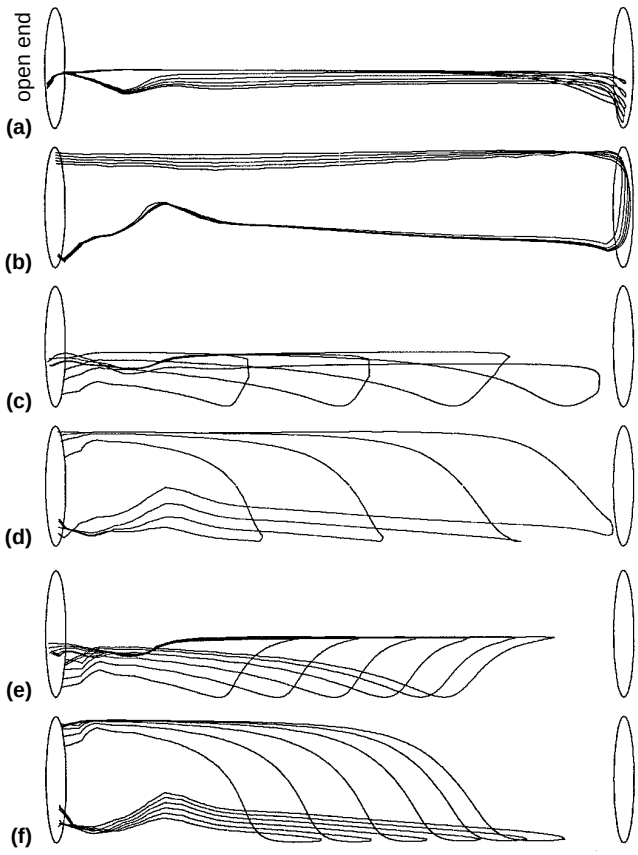

(a) top view, central vertical plane, **(b)** side view, central vertical plane,
(c) top view, side wall flow, **(d)** side view, side wall flow,
(e) top view, bottom wall flow, **(f)** side view, bottom wall flow.

Figure 4.
Particle tracks for uniform wall heating, $Ra = 10^6$, $L/R_0 = 10$

The effects of heating from the lower wall are manifested through disturbance of the separate flow streams near the orifice where a splitting of the tracks may be seen, and upward flow from the lower regions of the cylinder.

The interference near the orifice will be discussed in the section on "entrance effects". The upward flow along the curved wall occurs along the length of the cylinder as a consequence of uniform heating. An annular ring of rising fluid is formed near the walls while an eccentric core of cool fluid sinks in the middle. While at low Ra bifilamental flow was predominant, at higher Ra the flow may be said to have both bifilamental and annular characteristics (see Figure 5). Flow of a similar kind was also observed by Lock and Zhao (1990) in their numerical simulation of an inclined open thermosyphon with a rectangular cross-section, at low Rayleigh numbers.

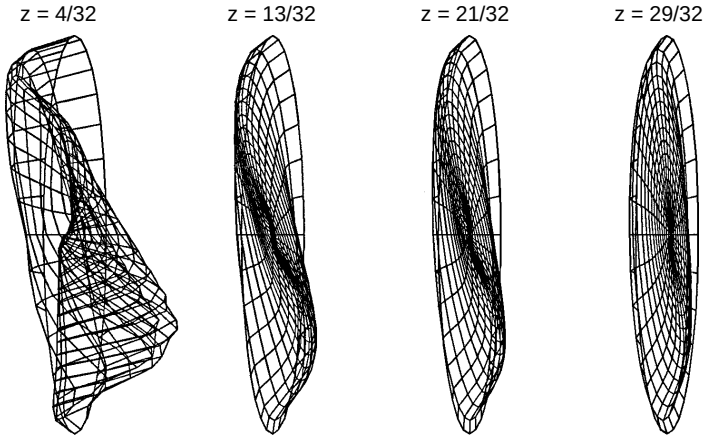

Figure 5.
Three-dimensional contour plots of axial velocity along the cylinder, uniform wall heating, $L/R_0 = 10$, $Ra = 10^5$

Martin and Cresswell (1957) observed that if an open thermosyphon is gradually inclined from the vertical then the Nusselt number at the walls decreases initially and then rises again to its original value when it reaches an inclination of 45°. In the vertical position flow was completely annular while at 45° flow was bifilamental. In between the two positions, a number of unstable states may be found which tend to promote mixing between the hot and cold streams and consequently reduce heat transfer.

Entrance effects

The boundary conditions used for the orifice allow one to calculate the distribution of velocity and temperature. The result shows cool inflow on the lower half of the orifice and warm outflow on the upper half. The cross-sectional distribution between the two opposing streams is not equal since the outgoing stream tends to travel at higher velocities.

For an open vertical thermosyphon there is considerable interference at the orifice, however, no such interference was observed at the orifice of the inclined differentially heated tube. For the uniformly heated cylinder, however, the rising fluid layers from the lower wall may be seen to interfere with the incoming cold stream at the orifice, causing part of that cold stream to short circuit back to the reservoir. One immediate effect of the interference is the splitting of the cold stream into two, as may be seen in Figure 6. The cold stream from the reservoir still enters through the lower section but peaks in two places on either side of the central vertical plane.

Differential wall heating mode

Like the uniform wall heating mode the flow is predominantly bifilamental, being made up of a U-loop over a wide range of Rayleigh numbers. The flow is, however, more stable than for uniform heating. In this configuration there are

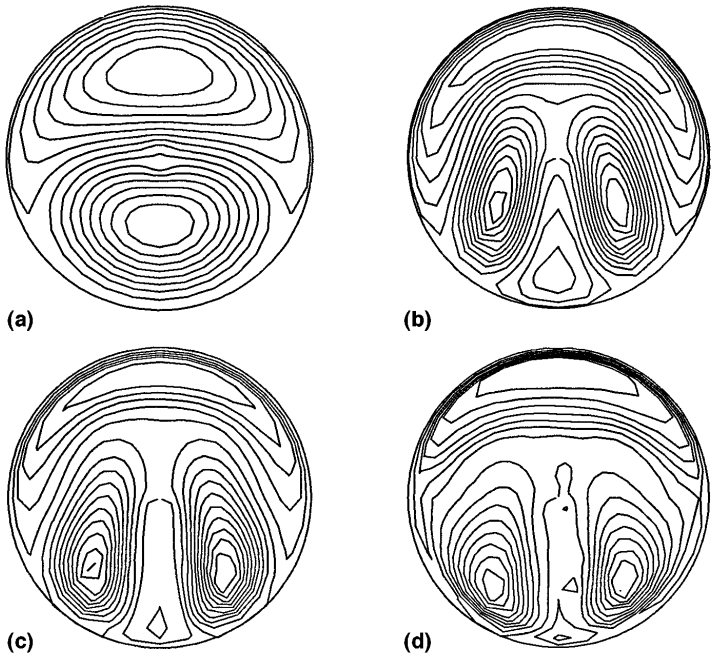

Figure 6.
Axial velocity contours at the orifice, $L/R_0 = 10$. (a) $Ra = 10^3$, (b) $Ra = 10^4$, (c) $Ra = 10^5$, (d) $Ra = 10^6$

no interfering streams generated near the orifice and impedance between the opposing currents is minimised.

The mass flow rate passing through the thermosyphon was calculated by numerically integrating the negative axial velocity component out of the tube over the area of the orifice. This is plotted as a function of Rayleigh number in Figure 7. It is evident that the fluid goes through a transition between Rayleigh numbers of 10^5 and 10^6. Up until 10^5 the development is gradual and smooth, but above 10^5 secondary flows begin to emerge and fluid turnover goes through a rapid increase.

Heat transfer results

For the purpose of heat transfer calculation, correlations are obtained for the Nusselt number. Early analytical work like Lighthill (1953) employed simplified models for the calculation of the Nusselt number. By assuming that the boundary layer thickness is very small compared with the radius of the cylinder Lighthill was able to show that the heat transfer may be modelled in a manner similar to that of a flat plate, that is

$$Nu = C_1 t_1^{1/4} \tag{20}$$

where t_1 is RaR_0/L and C_1 is a constant. For the present numerical work the Nusselt number is calculated from the temperature distribution solution as follows,

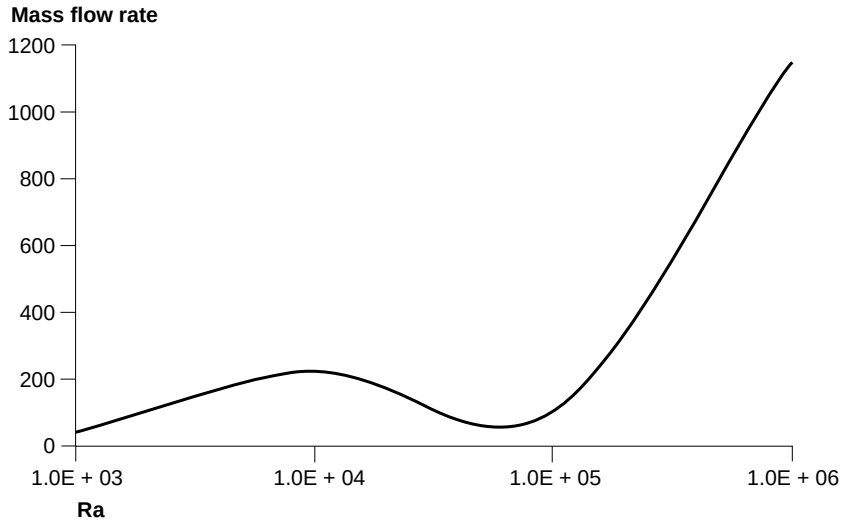

Figure 7.
Mass flow rate (non-dimensional) vs. Rayleigh number, for differential wall heating, $L/R_0=10$

$$Nu = \frac{1}{4\pi\left(L/R_0\right)} \int_0^{L/R_0} \int_0^{2\pi} \frac{\partial \theta}{\partial r}\, dz\, d\phi \tag{21}$$

Leslie (1960) analytically solved the problem of an inclined open thermosyphon, but his solution is limited to small angles of inclination. His work is, however, the only one of its kind and will therefore be used here for comparison, even though the range of Ra, aspect ratio and angle of inclination are beyond those that he specified for an accurate determination of Nusselt number. His correlation is

$$Nu = \frac{8}{3}\left(\frac{t_1}{240}\right)^{1/4}\left(1 + 0.0017\,\varepsilon^{2}\right) \tag{22}$$

where $\varepsilon = (L/R_0)\tan\gamma$, and γ is the angle of inclination from the vertical.

Martin and Cresswell (1957) and Hasegawa *et al.* (1963) experimentally investigated the open thermosyphon in its inclined and vertical forms respectively. Relevant selections from their results are also presented for comparison.

It may be seen from Figures 8 to 10 that Leslie's analysis gives a consistently higher Nusselt number than either Hasegawa's experimental results or the present numerical predictions. Leslie and Lighthill based their perturbation solutions on the assumption that Pr approaches infinity, which in the boundary layer regime could be expected to give slightly higher Nu values than for Pr = 1. Lighthill deliberately ignored the inertia terms in the momentum equation by making such an assumption. Leslie qualified his claims for accuracy by limiting

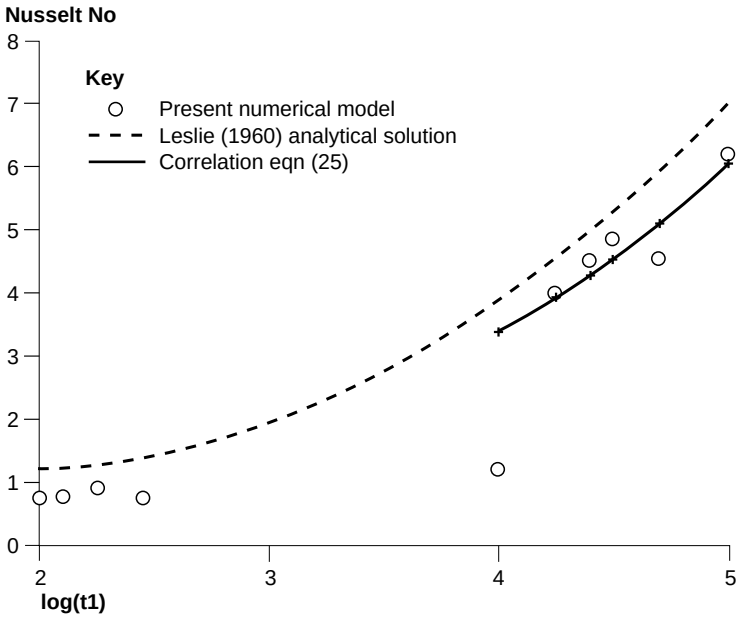

Figure 8.
Nusselt number as function of t_1, for differential wall heating

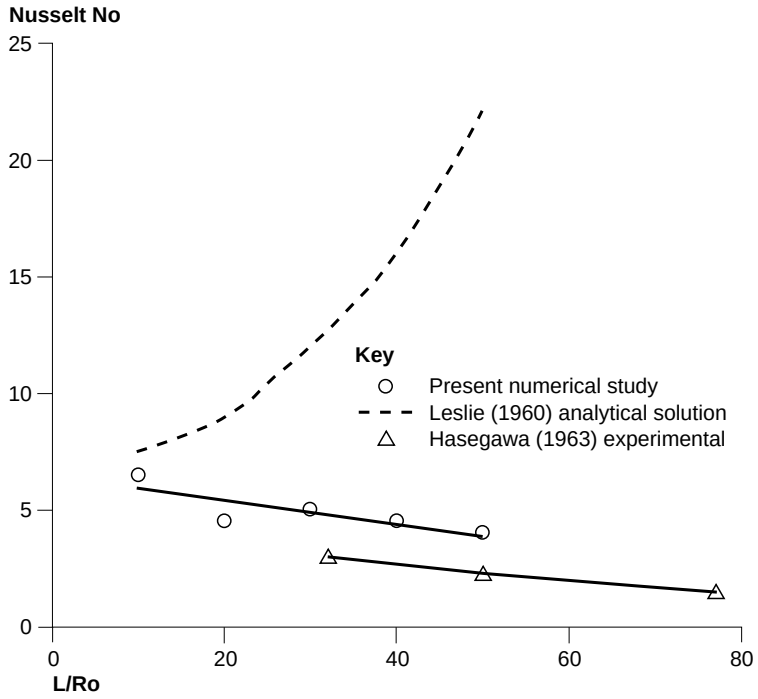

Figure 9.
Nusselt number as function of aspect ratio, for differential wall heating mode, $Ra=10^6$

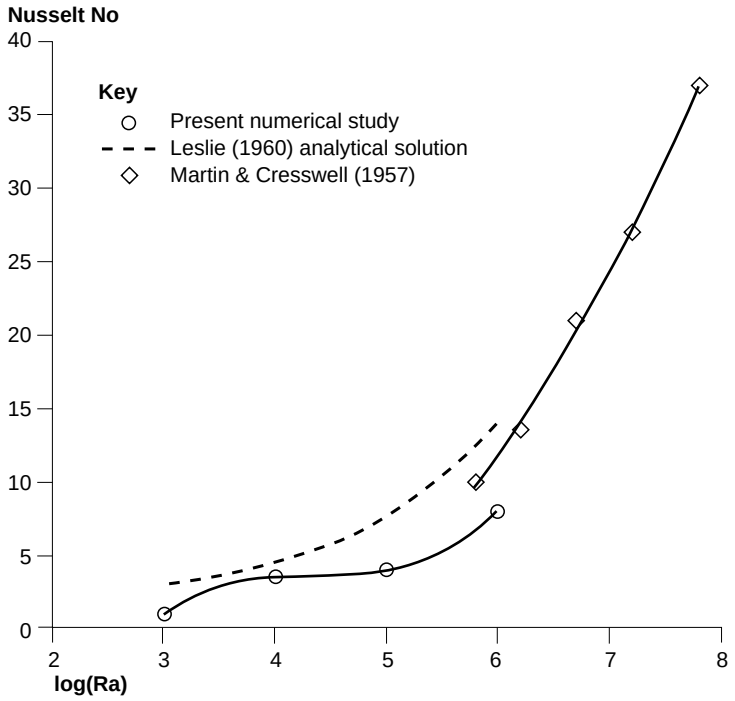

Figure 10.
Nusselt number as function of Ra for uniform wall heating

the applicability of his solution to small inclinations from the vertical. Lighthill completely ignored the azimuthal component of velocity since the boundary conditions on a vertical open thermosyphon were axi-symmetric, and performed integrations in the radial and axial directions only. Leslie included an azimuthal component in his analysis but its effect was limited to a few additional trigonometric functions. At small angles of inclination the flow is, by and large, annular, which is just like the vertical thermosyphon except for the slight eccentricity of the incoming flow, whereas flow at higher inclinations is predominantly bifilamental. Leslie's perturbation functions are essentially two-dimensional.

Martin and Cresswell's experimental results were determined for a higher range of Ra but there is an overlap at 10^6 (Figure 10). There is a qualitative agreement between their experimental results and the numerical results of the present work, as far as the trend is concerned. Leslie's results also show good agreement with the experimental and numerical results.

The abrupt transition of Nusselt number with t_1 observed in the present numerical at $t_1=10^4$ study (Figure 7) has previously been reported in several analytical, numerical and experimental investigations strongly implying instability in this region. Such instability is typically accompanied by oscillation in the orifice temperature, as observed experimentally by Hasegawa

et al. (1963). The oscillation was observed to subside as t_1 was increased further, and the flow entered into the bifilamental regime.

Secondary flows near the orifice have been associated with transition from impeded to boundary layer flow, but they have not been cited as being the cause of it. The effect of aspect ratio on the onset of transition has not yet been fully determined, however, its influence if any can only be secondary. The experimental investigations of Martin (1955) are unclear: certain substances, such as water, seem to be aspect ratio dependent, while others, such as air, are not. The factor most critical to transition is the Rayleigh number. If there is a critical value for the uniform heating mode, it would be between 10^4 and 10^5, when secondary flows emerges near the orifice and the Nusselt number plateaus. In the differential heating mode, the critical value will occur after Ra of 10^5 as shown in Figure 7. If Nusselt number is to be used as the criterion, then it may be seen that between Ra = 10^5 and 10^6 (i.e. between t_1 = 10^4 and 10^5 in Figure 8) there is a steep increase in heat transfer.

From the numerical results a correlation for uniform wall heating similar in form to that of Lighthill was obtained as follows:

$$Nu = 0.6\, t_1^{1/4} \tag{23}$$

The coefficient for uniform wall heating agrees favourably with figures developed by the early workers. Leslie gives 0.677 for a vertical cylinder filled with water and Squire (Goldstein, 1938) gives 0.654.

For differential wall heating a power function correlation of the above form can be fitted to high Ra number results, however, it does not match the low Ra results.

For Ra > 10^5

$$Nu = 0.34\, t_1^{0.25} \tag{24}$$

For Ra < 10^5 the Nusselt number seems to plateau at Nu= 0.95.

Experimental results

Figure 11 shows the velocity profiles on the central vertical plane for an aspect ratio of 10 and Ra from $7*10^5$ to $1.75*10^6$. The general shape of the profiles is the same for the range of aspect ratio considered and suggests that the flow near the orifice is essentially bifilamental, i.e. consisting of two main streams. Warm fluid exits through the upper half of the orifice after being heated by the cylinder walls. Cool fluid enters by way of replacement through the lower half of the orifice, descends down the tube then turns around and ascends while it is being heated along the walls.

Other evidence to show that flow in the inclined open thermosyphon is predominantly bifilamental was reported by Martin and Lockwood (1964) who showed through their flow visualisation work that two opposing streams can co-exist side by side in an inclined thermosyphon, with nothing but a naturally occurring boundary between them. Lock and Zhao (1990) numerically

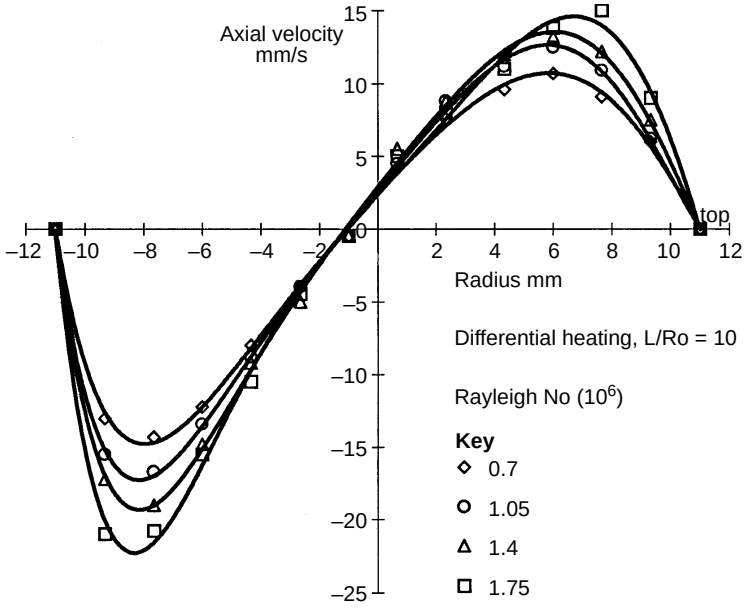

Figure 11.
Measured axial velocity profiles, differential wall heating, $L/R_0 = 10$

simulated flow inside an inclined open thermosyphon with a square section at low Ra, and found that the flow had both bifilamental and annular characteristics.

Numerical vs. experimental axial velocities

Figures 12 and 13 show a comparison of numerical and experimental orifice velocity profiles. For differential wall heating the numerical model over-predicts the maximum outgoing w-velocity by 20 per cent and over-predicts the maximum incoming velocity by 3 per cent. Although there is qualitative agreement between the two sets of results the numerical results generally show more significant variation of velocity across the diameter. For example, a sharper outgoing velocity peak and a thinner boundary layer on the upper wall. For both uniform and differential heating the incoming stream has a broader shape than the outgoing one.

For uniform wall heating the order of magnitude of the maximum velocity is similar, although the qualitative agreement is somewhat inferior compared to differential heating. The numerical model over-predicts the maximum outgoing velocity by only 1 per cent but under-predicts the incoming maximum velocity by 40 per cent. These results could be due to the discontinuity in the temperature boundary condition at the orifice assumed in the numerical model. In practice the discontinuity of temperature may be reduced owing to mixing in the supply reservoir immediately adjacent to the entrance of the cylinder. In the experimental test true uniform heating is difficult to achieve because of the divider between the upper and lower heating chambers, which allows some

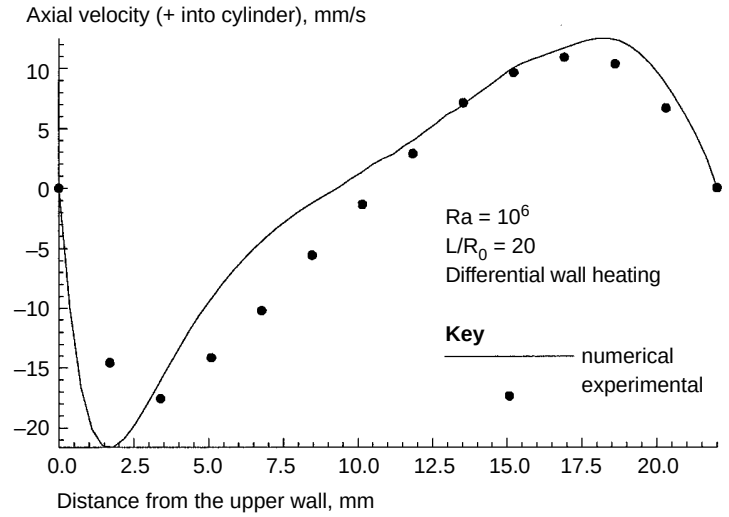

Figure 12. Axial velocity profiles, numerical vs. experimental results, DWH, $Ra = 10^6$, $L/R_0 = 20$

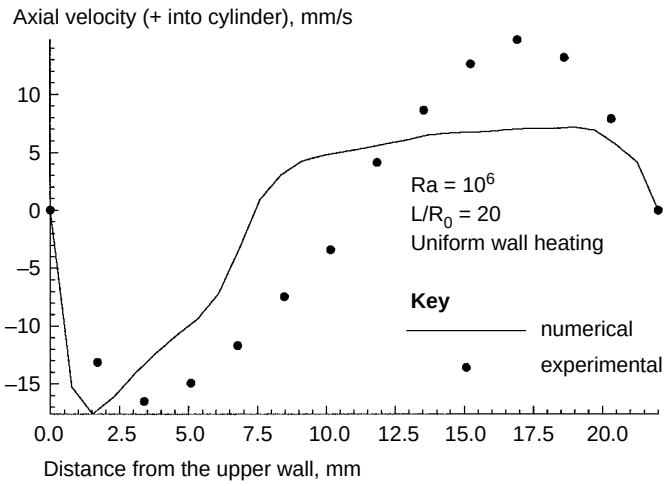

Figure 13. Axial velocity profiles, numerical vs. experimental results, UWH, $Ra = 10^6$, $L/R_0 = 20$

heat exchange between the two chambers. The temperature boundary condition along the cylindrical walls in the experimental rig may not have been isothermal as was assumed in the numerical model. The external heating chambers were isothermal as a result of the high heating water flow rate, however, owing to circumferential conduction in the glass walls the inner temperature boundary condition may have deviated from isothermal conditions. The absence of strong upward moving flow from the lower wall may be a consequence of the deviation of the experimental boundary conditions from isothermal conditions.

Numerical solutions of Lock and Zhao (1990) as well as the present numerical investigation predict significant flow rising from the bottom wall. Leslie's (1960) analytical model indicates this type of flow, and Martin and Cresswell (1957) demonstrated it experimentally in thermosyphons inclined at angles from 0° to 45°, and have cited this as the cause of the instabilities which made the Nusselt number dip for certain inclination angles.

Lock and Zhao (1990) predicted that annular flow occurs only for low inclinations and near the sealed end. The present numerical model showed the same but the extent of annular flow was seen to vary with the amount of heating applied.

Conclusion

The flow structure in an open thermosyphon inclined at 45° has been investigated experimentally and numerically. The investigation shows that flow in a differentially heated inclined open thermosyphon is typically bifilamental. A naturally occurring boundary was maintained between the cold and warm streams at all times. Using the classification of flows originally made by Lighthill, the flow would be called impeded for $Ra < 10^5$ or $t_1 < 10^4$, beyond which transition to boundary layer flow begins. Previous workers have quoted $t_1 = 10^{3.5}$ to $10^{3.8}$ as the region of transition for vertical open thermosyphons. The structure of flow for uniform wall heating is quite different than for differential wall heating. The flow starts out by being bifilamental at low Rayleigh number (10^3), very similar to the flow for differential wall heating, but as Ra is increased to beyond 10^5, an upward flow is developed from the bottom surface, making the flow annular.

The present work has confirmed previous experimental studies showing that the interference between incoming and outgoing fluid at the orifice potentially reduces heat transfer by disturbing the continuity of flow and by mixing, which narrows the effective temperature difference between the source and sink of heat in the thermosyphon. The velocity profiles measured by LDA confirmed the flow visualisation observations of Behnia *et al.*, who demonstrated the formation of distinct opposing streams in a thermosyphon in an inclined open cylinder.

References

Abib, A.H. and Jaluria, Y. (1988), "Numerical simulation of the buoyancy-induced flow in a partially open enclosure", *Numerical Heat Transfer,* Vol. 14, pp. 235-54.

Behnia, M., Morrison, G.L. and Paramasivam, S. (1987), "Heat transfer and flow in inclined open thermosyphons", ASME-JSME Thermal Engineering Joint Conference, Honolulu, Hawaii.

Chow, S.P., Harding, G.L., Yin Zhiqiang and Morrison, G.L. (1984), "Optimisation of evacuated tubular solar collector arrays with diffuse reflectors", *Solar Energy*, Vol. 33, pp. 277-82.

Goldstein, S. (Ed.)(1938), *Modern Developments in Fluid Dynamics*, Aeronautical Research Council of Great Britain, Oxford.

Hasegawa, S., Nishikawa, K. and Yamagata, K. (1963), "Heat transfer in an open thermosyphon", *Bulletin of the JSME,* Vol. 6, pp. 331-42.

Hirasaki, G.J. and Hellums, J.D. (1967), "A general formulation of the boundary conditions on the vector potential in three-dimensional hydrodynamics", *Quarterly Applied Mathematics*, Vol. 26, April, pp. 331-42.

Japikse, D. (1972), "Advances in thermosyphon technology", *Advances in Heat Transfer*, Vol. 19, Academic Press, Orlando, pp. 1-111.

Leong, S.S. (1981), "Natural convection in cylindrical containers", PhD Thesis, The University of New South Wales, Sydney, Australia.

Leslie, F.M. (1960), "Free convection in the tilted open thermosyphon", *Journal of Fluid Mechanics*, Vol. 7, pp. 115-27.

Lighthill, M.J. (1953), "Theoretical considerations on free convection in tubes", *Quarterly Journal of Mechanics and Applied Mathematics*, Vol. 6 No. 4.

Lock, G.S.H. and Zhao, L. (1990), "Effects of inclination on an air-filled open thermosyphon at low Rayleigh numbers", *ASME Heat Transfer Division (HTD) Publication*, Vol. 140, pp. 77-81.

Martin, B.W. (1955), "Free convection in an open thermosyphon, with special reference to turbulent flow", *Proceedings of the Royal Society, Series* A, Vol. 230, pp. 502-30.

Martin, B.W. and Cresswell, D.J. (1957), "Influence of coriolis forces on heat transfer in the open thermosyphon", *The Engineer*, Vol. 204, pp. 926-30.

Martin, B.W. and Lockwood, F.C. (1964), "Entry effects in the open thermosyphon", *Journal of Fluid Mechanics*, Vol. 19, pp. 246-56.

Wong, A.K. and Reizes, J.A. (1984), "An effective vorticity-vector potential formulation for the numerical solution of three-dimensional duct flow problems", *Journal of Computational Physics*, Vol. 55, pp. 98-114.

Yang, Y. and Camarero, R. (1986), "An improved vorticity-potential method for three-dimensional duct flow simulations", *International Journal of Numerical Methods in Fluids*, Vol. 6, pp. 35-45.

Further reading

Takeuchi, M., Kimura, T. and Higashikawa, Y. (1988), "Heat transfer in an open rectangular thermosyphon", (Thermosyphon passage with uniform temperature and adiabatic surfaces), *Journal of the Japanese Society of Machinery*, Vol. 54 No. 504, pp. 2090-98.